

Neutrinos from propagation of ultra–high energy protons

Ralph Engel, David Seckel and Todor Stanev

Bartol Research Institute, University of Delaware, Newark, DE 19716, USA

We present a calculation of the production of neutrinos during propagation of ultra-high energy cosmic rays as may be produced in astrophysical sources. Photoproduction interactions are modeled with the event generator SOPHIA that represents very well the experimentally measured particle production cross sections at accelerator energies. We give the fluxes expected from different assumptions on cosmic ray source distributions, cosmic ray injection spectra, cosmological evolution of the sources and different cosmologies, and compare them to the Waxman-Bahcall limit on source neutrinos. We estimate rates for detection of neutrino induced showers in a km³ water detector. The ratio of the local high energy neutrino flux to the ultra-high energy cosmic ray flux is a crucial parameter in distinguishing between astrophysical and cosmological (top-down) scenarios of the ultra-high energy cosmic ray origin.

98.70.Sa, 13.85Tp, 98.80.Es, 13.15.+g

I. INTRODUCTION

The highest energy cosmic rays are energetic enough to have photoproduction interactions on the microwave background. These collisions cause energy loss affecting the cosmic ray spectrum [1] – the GZK cutoff. In most astrophysical environments all secondary mesons produced in photoproduction interactions decay into γ -rays and neutrinos. Shortly after the original papers on the GZK cutoff it was suggested [2] that guaranteed fluxes of ultra-high energy (UHE) neutrinos will be produced by the propagation of UHE cosmic ray (UHECR) protons in the Universe. This suggestion was followed by more sophisticated estimates [3–7] that attempted to predict more realistically the expected neutrino fluxes and relate the detection of such fluxes to the neutrino cross section at very high energy and the then unknown mass of the W boson. Hill & Schramm [8,9] introduced the cosmological evolution of cosmic ray sources and used the measurements of the cosmic ray spectrum by the Haverah Park [10] and the Fly’s Eye [11] experiments to determine minimum and maximum allowed normalizations for the flux of such ‘propagation’ neutrinos and calculated detection rates for different types of detectors. More recent estimates include the work of Stecker and collaborators [12], Yoshida & Teshima [13], and Protheroe & Johnson [14].

Meanwhile the world statistics of ultra-high energy cosmic rays has significantly increased [15] and, most importantly, two events of energy substantially above 10²⁰ eV were detected by the Fly’s Eye [16] and AGASA [17] experiments. These events suggest that the maximum energy of cosmic ray acceleration E_{max} may be significantly higher than the previous nominal estimate of 10²⁰ eV, if these events are not a result of the decay of extremely massive exotic particles [18] or other exotic processes [19].

We assume that UHECR are of astrophysical origin and present here a new estimate of the expected neutrino fluxes generated during propagation by the ultra-high en-

ergy cosmic rays. We use recent results on the propagation of UHE protons [20] to estimate the neutrino production. The aim is to explore the neutrino production with a photoproduction interaction model (SOPHIA [21]) that fits well the experimentally measured multiparticle production data over a wide energy range. For this purpose we extend the calculation of proton propagation in the local universe by Stanev *et al.* [20] to cosmological distances. We also study the importance of the cosmological evolution of the sources of cosmic rays in different cosmological models. The aim of the present work is to study the level at which these ultra-high energy neutrinos are indeed guaranteed.

Section II discusses the neutrino production from propagation of ultra-high energy protons in the local Universe. In Section III we obtain the neutrino spectra from homogeneously distributed cosmic ray sources accounting for the cosmological evolution of these sources. Section IV explores variations in this flux under the influence of different assumptions concerning proton injection spectra, source evolution and distribution, and background cosmology. Section V gives a brief overview of the event rates that could be expected in future large neutrino detectors. Discussion of the results and the conclusions from this research are given in Section VI.

II. NEUTRINO FLUXES FROM PROTON PROPAGATION IN THE LOCAL UNIVERSE

We begin with our method for calculating neutrino production from proton propagation in the the nearby universe (for a detailed discussion see [20]). The calculation is carried out as a Monte Carlo simulation of individual particle histories in the presence of the cosmic background radiation, including energy loss processes such as photoproduction, e^+e^- pair production, and adiabatic losses. The extension of this method to cosmological distances is discussed Sec. III.

An important new ingredient of the calculation is to use the event generator SOPHIA [21] to simulate in detail the proton/neutron interactions with photons from the cosmic microwave background. This event generator

has several main differences from previously used codes: (1) the inclusion of direct pion production at the photo-production threshold. In this t -channel process the photon is absorbed via a $\gamma\pi^+\pi^+$ vertex, and so only charged pions are produced. Although the cross section for this process is smaller than the dominant Δ^+ resonance, it yields a significant number of neutrinos, when folded with the steep proton injection spectrum.

(2) explicit consideration of 10 different resonance production channels in the important energy region just above the particle production threshold.

(3) QCD motivated multipion production at large center-of-mass energies.

To evaluate the neutrino yields, protons are injected in narrow logarithmic bins and all products of their interactions are collected with the same energy binning. We use 10 bins per energy decade, and 10000 protons per bin weighted by an E^{-2} spectrum within each bin. The injection energy ranges from 10^{19} to 10^{23} eV. This gives the option to explore different injection power spectra and cutoff energies by rescaling the products of each energy bin.

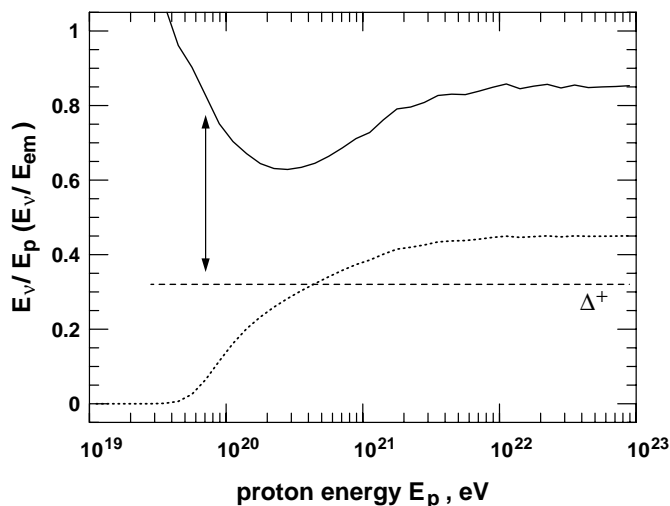


FIG. 1. Neutrino production efficiency, summed over flavors, as a function of proton injection energy. The solid curve shows the ratio of the energy carried by neutrinos to that of electromagnetic particles due to photoproduction in fully developed cascades (200 Mpc), as simulated with SOPHIA [21]. The dashed curve is the same ratio but for the Δ^+ resonance approximation which is frequently used in analytic calculations. The dotted curve shows the total neutrino energy relative to injected proton energy for SOPHIA.

The results from the Monte Carlo are illustrated in Fig. 1. Concerning the overall yield of neutrinos, the dominant feature is the turn on of the GZK process at $E_p \approx 5 \times 10^{19}$ eV. The ratio of yield in neutrino energy to yield in radiative energy depends primarily on the ratio of charged to neutral pion production. If all pion production occurred through the Δ^+ resonance approximation this ratio would be approximately $(\frac{3}{4} \times \frac{1}{3}) / (\frac{2}{3} + \frac{1}{4} \times \frac{1}{3}) = \frac{1}{3}$, where

for charged pions $\sim \frac{3}{4}$ of the energy goes to neutrinos. At high energies, isospin “democracy” suggests that the ratio should tend to $(\frac{3}{4} \times \frac{2}{3}) / (\frac{1}{3} + \frac{1}{4} \times \frac{2}{3}) = 1$. For low energy protons, direct production of charged pions plays an important role, again increasing the neutrino yield above that expected from the Δ^+ resonance.

The next step is to place the neutrino production model into an astrophysical setting. For the proton source spectra we use a power law with an exponential high-energy cutoff

$$\frac{dN}{dE} \propto E^{-\alpha} \times \exp(-E/E_c), \quad (1)$$

where $\alpha = 2$ unless otherwise stated and $E_c = 10^{21.5}$ eV. During propagation, adiabatic energy losses for the protons are calculated assuming $H_0 = 75$ km/s/Mpc. Similarly, neutrino energies are redshifted by a factor of $(1+z)$, where z is the redshift of the interaction site.

The energy degradation of ultra-high energy protons in propagation in the microwave background is very fast. The minimum mean free path for photoproduction interactions is 3.8 Mpc at a proton energy of $\sim 6 \times 10^{20}$ eV. Protons with an energy of about 10^{21} eV thus interact on the average twice or more during the first 10 Mpc of propagation and lose close to 50% of their injection energy. A significant fraction of the energy loss (about 40%) goes into neutrinos. The neutrino flux thus originates from the initial stages of proton propagation.

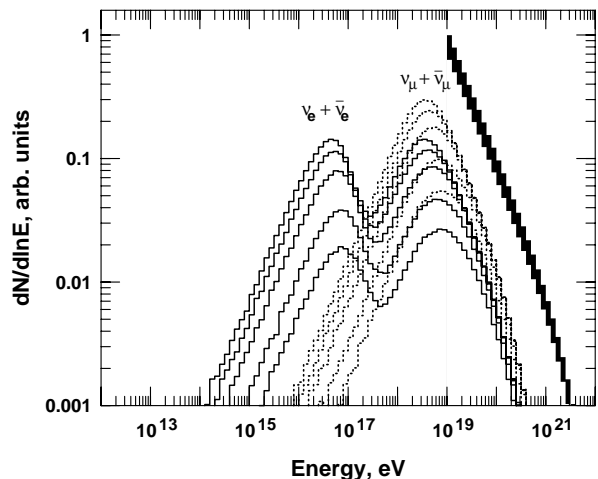


FIG. 2. Neutrino fluxes produced during the propagation of protons over 10, 20, 50, 100, and 200 Mpc (from bottom up) in a 1 nG random magnetic field. The heavy histogram shows the proton injection spectrum defined in Eq. (1).

Fig. 2 shows the fluxes of electron and muon neutrinos after propagation over different distances up to a maximum of 200 Mpc. About 60% of the final neutrino fluxes are generated in the first 50 Mpc and more than 80% in the first 100 Mpc. The contribution from the second half of the maximum propagation distance is small because the proton spectrum is deprived of $> 10^{20}$ eV particles

and photoproduction interactions are rare. It follows, therefore, that from the point of view of neutrino production a source at 200 Mpc produces a fully evolved spectrum. Accordingly, for the cosmological scenarios that follow in Section III we scale the neutrino yields to this result.

There are two other noticeable features in the neutrino spectra shown in Fig. 2. The muon neutrino spectra have a single peak at energies between 10^{18} and 10^{19} eV. Electron neutrinos, however, exhibit a more complicated double peak structure. The first peak between 10^{16} and 10^{17} eV is populated by $\bar{\nu}_e$ from neutron decay. The neutron decay length equals the photoproduction interaction length at about 4×10^{20} eV and neutrons of lower energy are more likely to decay than to interact. This leads to the formation of an additional peak in the electron neutrino spectrum. The second peak, in a position similar to that of muon neutrinos, is populated mostly by ν_e from μ^+ decay with a small admixture of $\bar{\nu}_e$ generated predominantly in neutron photoproduction interactions. The ratio of $(\nu_\mu + \bar{\nu}_\mu)/(\nu_e + \bar{\nu}_e)$ in the second peak is 2, as expected, although integrated over the whole spectrum the ratio is closer to 1.

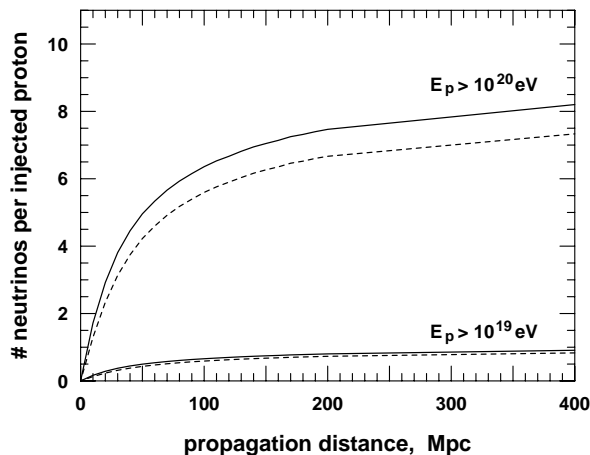


FIG. 3. Total number of neutrinos produced per injected proton of energy above 10^{19} eV (lower curves) and 10^{20} eV (upper curves). The proton energy was sampled from the spectrum (1). Solid lines show the sum of muon neutrinos and antineutrinos, the dashed lines are for electron neutrinos and antineutrinos.

One also notices the slight shift of the peak of the distribution to lower energy with the propagation distance. At longer propagation distance, lower energy protons suffer photoproduction interactions and generate lower energy neutrinos. There is also a small effect from the adiabatic losses of all neutrinos, but this is hardly noticeable here because the maximum source redshift considered is only $z \approx 0.05$.

Fig. 3 shows the total number of neutrinos produced per source proton as a function of the source distance. Because the protons lose most of their energy during

propagation over the first 50 Mpc, one would naively expect that the neutrino number does not change for source distances above 100 Mpc. The continuing rise of the neutrino to proton number ratio is due to redshift effects. The minimum proton energy for photoproduction interactions decreases as $(1+z)^{-1}$, which leads to an increase of the number of interacting protons. Even for relatively small redshifts involved ($z = 0.1$ for 400 Mpc) this leads to an increase of the generated number of neutrinos.

Fig. 3 also underlines the importance of the maximum energy of the proton injection spectrum. In this calculation we use an exponential cut-off with $E_c = 10^{21.5}$ eV. Assuming an E_c of $10^{20.5}$ eV would not drastically decrease the neutrino flux. Cutting off the proton injection spectrum at lower energy would, however, require very nearby sources for the extremely high energy showers detected by the Fly’s Eye and AGASA experiments.

III. NEUTRINOS FROM PROTON PROPAGATION OVER COSMOLOGICAL DISTANCES

In the following we will focus on the case of uniformly distributed sources with identical proton injection spectra. Although a homogeneous source distribution is disfavored by the resulting source energy requirements and arrival proton spectra [19,22], it serves here as a simple generic model whose results can be easily rescaled to account for local density enhancements or even nearby point sources.

The local neutrino flux of flavor i generated from the propagation of cosmic rays over cosmological distances can be written as an integral over redshift and the proton energy E_p^s (s denotes “source”)

$$\mathcal{F}_i(E_{\nu_i}) = \frac{c}{4\pi E_{\nu_i}} \int \int \mathcal{L}(z, E_p^s) Y(E_p^s, E_{\nu_i}, z) \frac{dE_p^s}{E_p^s} dz. \quad (2)$$

Here, the neutrino yield function is

$$Y(E_p^s, E_{\nu_i}, z) = E_{\nu_i} \frac{dN_{\nu_i}}{dN_p dE_{\nu_i}}. \quad (3)$$

Also, the source function per unit redshift is

$$\mathcal{L}(z, E_p^s) = \mathcal{H}(z) \eta(z) \mathcal{L}_0(E_p^s), \quad (4)$$

where $\mathcal{H}(z)$ parametrizes the cosmological source evolution, $\eta(z)$ describes the cosmological expansion, and $\mathcal{L}_0(E_p^s)$ is a properly normalized version of the source spectrum in Eq. (1). The metric element $\eta(z)$ is defined as

$$\eta(z) = \frac{dt}{dz} = \frac{1}{H_0(1+z)} [\Omega_M(1+z)^3 + \Omega_\Lambda + (1 - \Omega_M - \Omega_\Lambda)(1+z)^2]^{-1/2} \quad (5)$$

which simplifies to $1/(H_0(1+z)^{5/2})$ for the Einstein – de Sitter universe ($\Omega_M = 1, \Omega_\Lambda = 0$).

The yield function Y is evaluated utilizing the Monte Carlo result for a 200 Mpc source and the scaling relation

$$Y(E_p^s, E_\nu, z) = Y((1+z)E_p^s, (1+z)^2 E_\nu, 0). \quad (6)$$

In scaling E_ν one factor of $(1+z)$ arises from redshifting the neutrino energy from its observed value to its production value. Both E_ν and E_p^s scale by $(1+z)$ to maintain the same invariant reaction energies in the presence of a higher cosmic background temperature. Although it simplifies the numerical work considerably, utilizing the scaling relation introduces some approximations. For redshifts $\lesssim 0.05$ it overestimates the neutrino production as per Fig. 2. However the contribution to the total fluxes coming from $z < 0.05$ is very small (see Fig. 5 below). Another effect is that at high redshift the competition between neutron decay and neutron photoproduction is altered in favor of photoproduction, and so we make a modest overestimate of the $\bar{\nu}_e$ flux around 10^{16} eV. At high energies, the sum of $\bar{\nu}_e$ and ν_e fluxes remains unchanged, but the flavor distribution may be altered.

The source proton luminosity \mathcal{L}_0 is parametrized as

$$\mathcal{L}_0(E_p^s) = P_0 \left(\int_{E_{\min}}^{E_{\max}} E_p^s \frac{dN_p}{dE_p^s} dE_p^s \right)^{-1} E_p^s \frac{dN_p}{dE_p^s}, \quad (7)$$

with dN_p/dE_p^s given by Eq. (1) and P_0 denoting the injection power per unit volume.

The injection power of cosmic rays with energy above $E_{\min} = 10^{19}$ eV can be roughly estimated using the local cosmic ray energy density [23]. The cosmic ray flux $dN/(dEd\Omega dAdt)$ at 10^{19} eV is about 2.5×10^{-28} $\text{cm}^{-2}\text{s}^{-1}\text{ster}^{-1}\text{GeV}^{-1}$. Assuming that:

- 1) all cosmic rays at that energy are extragalactic;
- 2) 10^{19} eV cosmic ray flux is as at injection; and
- 3) the differential proton spectrum at injection is a power law with spectral index $\alpha = 2$,

one obtains a cosmic ray energy density

$$\rho_e = \frac{4\pi}{c} \int E \frac{dN}{dEd\Omega dAdt} dE \quad (8)$$

of 1.1×10^{54} erg/Mpc³ per decade of energy. To calculate the injection power required to maintain this energy density one needs to make an assumption about the lifetime τ_{CR} of these cosmic rays. A conservative approach would be to use a lifetime close to the Hubble time. Using $\tau_{CR} = 10^{10}$ yrs gives a power of 1.1×10^{44} erg/Mpc³/yr per decade of energy. Of course, the total power for $E > 10^{19}$ eV depends on the maximum energy at acceleration.

The correct way of calculating the injection power for a model of cosmic ray source distribution and injection (acceleration) spectra is to propagate the accelerated spectra from the sources to us and fit the locally observed spectrum. We do not perform this procedure because it

involves assumptions on the cosmic ray source distribution and the structure and strength of the extragalactic magnetic fields which are beyond the scope of this paper. We use instead the cosmic ray injection power obtained in a similar, somewhat simplified way by Waxman [24], who derived $P_0 = 4.5 \pm 1.5 \times 10^{44}$ erg/Mpc³/yr between 10^{19} and 10^{21} eV for power law cosmic ray injection spectra with α between 1.8 and 2.7. We will use this value of P_0 for the energy spectrum of Eq. (1) integrated between 10^{19} and 10^{22} eV. The higher E_{\max} approximately compensates for the factor of $\exp(-E/E_c)$ as compared to Waxman’s result.

Finally, we have to specify the cosmological evolution of the cosmic ray sources, $\mathcal{H}(z)$. We use the parametrization of [24], i.e.

$$\mathcal{H}(z) = \begin{cases} (1+z)^3 & : z < 1.9 \\ (1+1.9)^3 & : 1.9 < z < 2.7 \\ (1+1.9)^3 \exp\{(2.7-z)/2.7\} & : z > 2.7 \end{cases} \quad (9)$$

where $n = 3$ describes the source evolution up to moderate redshifts. We also briefly consider a stronger evolution model with $n = 4$ up to $z=1.9$ and flat at higher redshifts.

Fig. 4 shows electron and muon neutrino fluxes obtained with our nominal choice of astrophysical and cosmological parameters, and carrying out the integration to a redshift of $z_{\max} = 8$. Integrating to infinity increases the neutrino fluxes by only about 5%.

Fig. 4 also shows the limits on neutrino production in cosmic ray sources derived by Waxman & Bahcall [25,26] (WB). As those calculations were carried out for the same source evolution model, similar spectra and the same injection power P_0 , they serve to compare the expectations for ‘source’ versus ‘propagation’ neutrinos associated with UHECR of astrophysical origin. Our propagation flux is slightly below the WB limit for the muon neutrino and antineutrino flux for energies between 10^{18} and 10^{19} eV. The differences lie in the assumed neutrino yield per proton. For their limit, WB assume a maximal thin source, i.e. an energy equal to that of the injected proton is deposited into neutrinos, whereas for our calculation only a fraction goes into neutrinos, as shown in Fig. 1. At higher energies one can see the effect of the factor $\exp(-E/E_c)$ in our source spectrum. At lower energies, the cosmic background radiation is devoid of high energy photons and so low energy protons do not produce neutrinos. In contrast, the cosmic ray sources are assumed to have abundant higher energy photons and so the limit on source neutrinos continues to scale as E^{-2} to low energies.

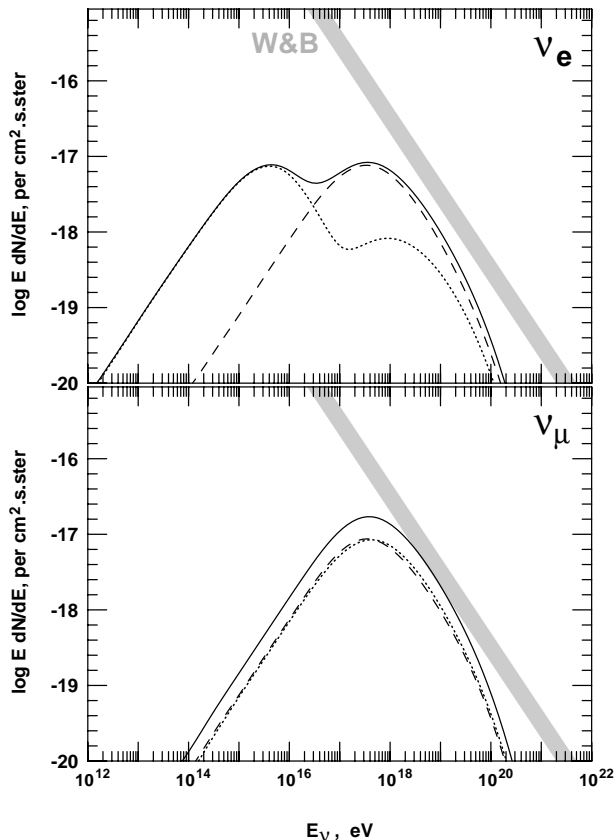


FIG. 4. Fluxes of electron neutrinos (dashed lines) and antineutrinos (dotted lines) generated in propagation of protons are shown in the upper panel. The lower panel shows the fluxes of muon neutrinos and antineutrinos. Solid lines show the sum of neutrinos and antineutrinos. The shaded band shows the Waxman & Bahcall [25,26] limit for neutrino production in cosmic ray sources with the same injection power. The lower edge of the band is calculated without account for the cosmological evolution and the upper one with the evolution of Eq. (9).

Fig. 5 is designed to show how the neutrino flux is built up from contributions at different redshifts. It is evident that the high and low ends of the neutrino spectrum are sensitive to different epochs of the source evolution. First consider the protons that will contribute to neutrinos with energy 10^{19} eV. At $z = 0$ these protons have an energy of a few times 10^{20} eV, above the threshold for photoproduction. This energy will increase with the source redshift. As a result, the source contribution $E_p dN/dE_p$ for these neutrinos effectively decreases as $(1+z)^{-1}$. To this we must add additional factors of $\eta(z)\mathcal{H}(z) \sim (1+z)^{0.5}$ for the source evolution in a $\Omega_M = 1$ cosmology, and a factor of $(1+z)$ explicit in the $(1+z)d/d(1+z)$ plot. Together, the function plotted naively scales as $(1+z)^{0.5}$. This scaling stops at $z = 1.9$ where $\mathcal{H}(z)$ is assumed to flatten. For higher energy neutrinos $E_\nu = 10^{20}$ eV, the increasing proton energy runs into the exponential cutoff E_c of our model injection spec-

trum causing a further decrease with $1+z$. The result of these considerations is that the highest energy neutrinos are produced primarily by relatively young sources, and are sensitive to assumptions about the recent universe.

For low energy neutrinos, say 10^{16} eV the story is a bit more complicated. From kinematic arguments the prime production candidate for such neutrinos would be a proton of energy a few times 10^{17} eV, but such protons are below the photoproduction threshold. Protons with higher energy can, of course, produce low energy neutrinos, but due to the small phase space the production is suppressed by a factor of E_ν/E_p . Now, as the source redshift increases, E_ν at production also increases as $1+z$. At the same time, the minimum value for E_p at production *decreases* due to the increasing cosmic microwave background temperature. Thus, phase space considerations of the neutrino production process yield a net factor of $(1+z)^2$. With the lowering of E_p , the source spectrum factor yields an increase of $1+z$. Including $\eta(z)\mathcal{H}(z)$ and the explicit $1+z$ for the plot gives an overall dependence of $(1+z)^{4.5}$ at low energies. This behavior continues until

- a) the source evolution model changes its z dependence, or
- b) the photoproduction threshold at z has dropped so that there is no phase space suppression for that neutrino energy. At that point there is a transition to the high energy behavior outlined above. The net result of these considerations is that the low energy part of the spectrum is dominated by high redshift sources, and is sensitive to assumptions of a cosmological nature in our calculation.

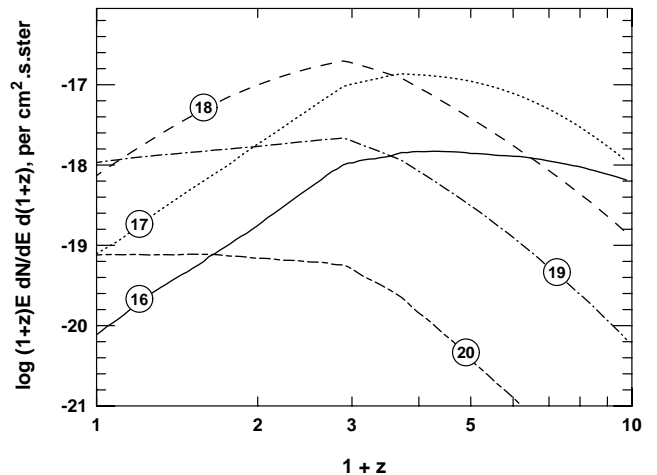


FIG. 5. The curves, labeled by $\log_{10}(E_\nu)$, show the contribution of different source distances to the neutrino flux as a function of redshift for our nominal $n = 3$ source evolution model given in Eq. (9).

Finally, we comment on the energy where the neutrino flux peaks in Fig. 4. Given the turn on of photoproduction (Fig. 1) and the kinematics of the Δ resonance, one might expect the peak to occur at around 10^{19} eV.

Our Monte Carlo, however, yields more neutrinos with a softer spectrum than a Δ resonance model, so the peak from a low redshift source occurs at about 3×10^{18} eV, as seen in Fig. 2. Moreover, as discussed just above, the peak of the cosmological spectrum is shifted by two factors of $(1+z)$ from the redshift which dominates the source contributions. For our \mathcal{H} , η and \mathcal{L}_0 this occurs at $(1+z) = 2.9$, and so the resultant neutrino spectrum peaks at around 3×10^{17} eV as seen in Fig. 4.

IV. VARIATIONS

Many of the parameters associated with the calculation of the neutrino fluxes shown in Fig. 4 have rather large uncertainties. The power needed to maintain the flux of cosmic rays above 10^{19} eV varies by about 30% for injection differential spectral indices between 1.8 and 2.7 [24]. The cosmological evolution of the source luminosity evaluated from star formation regions [27] could be somewhat stronger, as also indicated by the attempts to derive the cosmological evolution of GRB [28] and their fluences [29]. We show the influence on the generated neutrino fluxes in Fig. 6 where we calculate the neutrino flux with the same injection power but a stronger cosmological evolution - $(1+z)^4$ up to $z = 1.9$ and constant thereafter. The stronger cosmological evolution increases the neutrino flux by a factor of 3 and generates a small shift of the maximum flux to lower energy. The integration was carried again to redshift of 8.

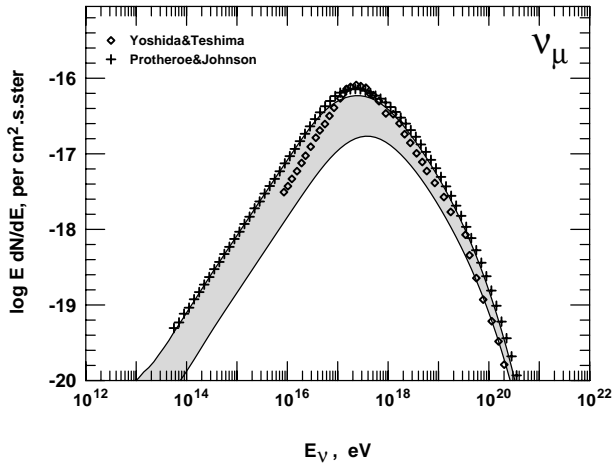


FIG. 6. The lower boundary of the shaded area corresponds to the neutrino flux shown in Fig. 4 with the source evolution $n = 3$ and the upper boundary is for $n = 4$ up to $z = 1.9$ and constant afterwards. Open diamonds show neutrino fluxes calculated by Yoshida and Teshima [13] and the crosses are due to Protheroe and Johnson [14].

The two sets of points in Fig. 6 represent calculations of Yoshida & Teshima (diamonds, source evolution with $n = 4$ and cutoff at $z = 4$) and of Protheroe & Johnson [14]

(crosses, energy cutoff at $E = 10^{21.5}$ eV).

All three calculations show the peak of the neutrino spectrum at approximately the same energy of $2-3 \times 10^{17}$ eV. The spectrum of Yoshida & Teshima is somewhat narrower than the one obtained in this work, while the agreement with Protheroe & Johnson is very good. This latter work uses the cosmological evolution evolution model RLF2 [30] with the ‘fudge factor’ of Rachen & Biermann [31] rather than a simple redshift dependence.

The neutrino flux calculated by Stecker *et al.* [12] (not shown) seems to be based on an injection power not much different from the normalization of Waxman. The spectrum however peaks at higher energy. An error might have been made in accounting for the neutrino redshift (F.W. Stecker, private communication).

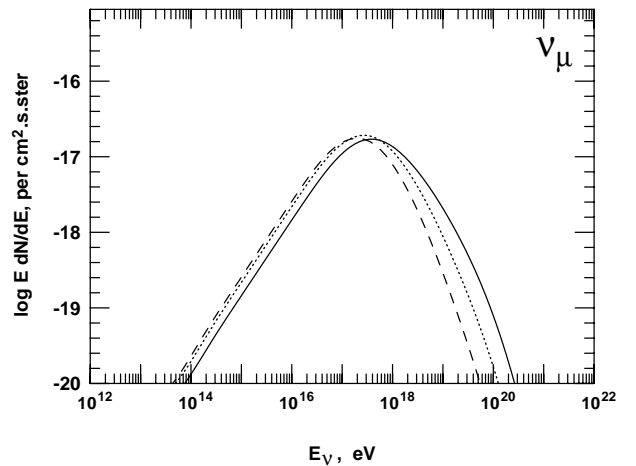


FIG. 7. Variation of neutrino flux resulting from different proton injection spectra. The dotted curve is for an injection spectrum of $E^{-2.5}$ and the dashed curve is for E^{-3} .

In Fig. 7 we show the neutrino fluxes obtained with the source evolution of Eq. (9) and differential injection spectral indices of 2.5 and 3, keeping again the injection power and E_c constant. The steeper injection spectra generate smaller neutrino fluxes at high energy, because of the much smaller number of protons above 10^{20} eV that are mostly responsible for high energy neutrino production. By contrast, low energy neutrinos are predominately generated by protons injected at high redshift, where the threshold for photoproduction is decreased by a factor of $1+z$. Because the total injection power is kept constant, a steeper spectrum results in an increase in the flux of lower energy protons and, hence, low energy neutrinos.

All results shown above are calculated for a homogeneous source distribution. It has been suggested in the past, and recently in the context of a specific acceleration model in Ref. [32] that the observed cosmic ray spectrum can be best fit by a combination of a homogeneous source distribution with an enhancement of local sources at distances less than 20 Mpc or with a single

source at a similar distance.

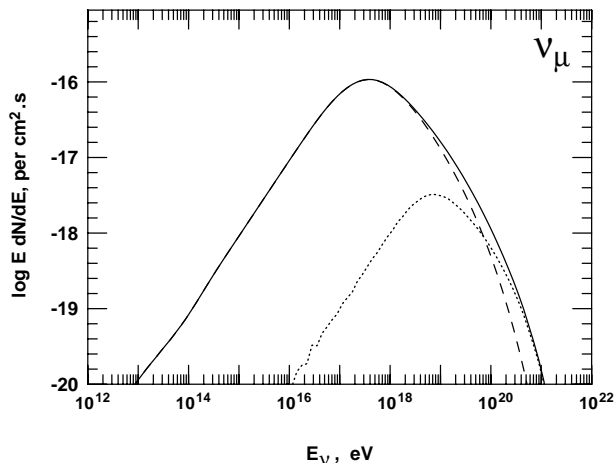


FIG. 8. Muon neutrino and antineutrino fluxes generated if one half of the local cosmic rays are generated by nearby sources at a distance of 20 Mpc. Note that fluxes are given for the full solid angle of 4π . The dashed curve corresponds to one half of the muon neutrino flux of Fig. 4, integrated over the full solid angle. The dotted line shows the production by locally generated cosmic rays by either a single source or by a local enhancement of the cosmic ray sources.

Fig. 8 shows the neutrino fluxes generated under the assumption that the injection power of homogeneously distributed sources is $P_0/2$ and 50% of the UHECR at 10^{19} eV are generated by a single source at a distance of 20 Mpc. This scenario will not predict a proton arrival spectrum similar to that of Waxman [24] because the injection spectrum is kept, up to the normalization, the same for the single source at 20 Mpc and the homogeneously distributed sources. It merely serves as a simple example of the changes to be expected in such a case. It is also a good approximation for a local density enhancement because the difference between the neutrino flux magnitudes for a single source and local enhancement scenarios is very small.

The observational difference is substantial because, for a single source scenario, most of the high-energy neutrinos would come from the direction of that source. Most of the neutrinos due to proton propagation from a local source would be generated in the first interaction of protons of energy above 10^{20} eV (see Fig. 3). These high-energy protons do not scatter significantly in a random extragalactic field with an average strength of less than 100 nG and the relativistic decay kinematics ensures that the neutrinos are emitted in the direction of the proton momentum.

Finally we discuss the importance of the cosmological model. All calculations shown above are performed with the assumption of a flat, mass dominated universe ($\Omega_M = 1$). However, recent astrophysical observations agree better with models containing a cosmological constant Λ [33]. From the behavior of η (see Eq. (5)) one may

expect an increased contribution to the neutrino production from higher redshifts.

Fig. 9 shows the difference in the expected neutrino fluxes for the Einstein – de Sitter Universe (solid line) and a model with $\Omega_M = 0.3$ and $\Omega_\Lambda = 0.7$, as currently favored by measurements [34], both with a source evolution proportional to $(1+z)^4$. We use the stronger source evolution and carry the integration out to a redshift of 8 to emphasize the difference between the cosmological models. For a flat universe the ratio of fluxes is always smaller than $1/\sqrt{1-\Omega_\Lambda}$ (see Eq. (5)). The difference between the Einstein – de Sitter Universe and one with a non-vanishing cosmological constant does not, however, depend very strongly on the cosmological evolution model of the sources. The ratio between the two cosmologies is about 1.6 for $n = 3$ evolution and 1.7 for $n = 4$ evolution.

We caution that in the absence of a model which consistently accounts for the effects of Ω_Λ on the source evolution function $\mathcal{H}(z)$, this increase should be regarded as an upper limit. Specifically, we have varied η , but kept \mathcal{H} constant, whereas it might be argued that keeping the product $\eta\mathcal{H}$ constant would be a better approximation to the effects of a non-zero Ω_Λ on the source evolution, in which case there would be no change in the neutrino flux.

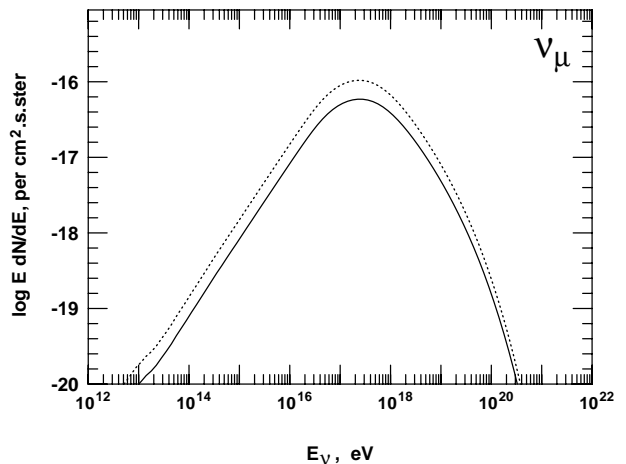


FIG. 9. Muon neutrino and antineutrino fluxes from homogeneous source distribution for the Einstein – de Sitter Universe (solid line) and for $\Omega_\Lambda = 0.7$ (dashed line), using a cosmological evolution of $(1+z)^4$ up to redshift of 1.9 and flat at higher redshifts.

V. EVENT RATES FROM THESE NEUTRINOS

Detection of neutrinos produced during the propagation of UHECR protons is a challenge. The flux peaks above 10^{17} eV where the neutrino nucleon cross-sections are of order 10^{-31} cm². Such values of $\sigma_{\nu N}$ are large enough to make the Earth opaque, but still require 100-

1000 km of water to ensure an interaction. As a result, there is no sensitivity to upward neutrinos and low efficiency for downward neutrinos. Under these circumstances the prime detector requirement is large mass, of order 100 km^3 (water), in order to guarantee a few events per year. With such large volumes, the typical event may be assumed to be a contained event where the visible energy is dominated by the high energy shower associated with the neutrino interaction vertex. Special detector geometries may provide additional sensitivity to μ or τ leptons produced in charge current events. Although we phrase our discussion in terms of water/ice detectors, sufficient mass may also be achieved by monitoring large volumes of atmosphere.

All types of neutrino interactions generate showers. In charged current (CC) interactions of electron neutrinos and antineutrinos the neutrino energy is completely released in the form of shower particles. The hadronic shower carries a fraction y of the initial neutrino energy E_ν , while the electromagnetic shower carries the remaining $(1-y)E_\nu$. Although the electromagnetic shower will be stretched out by the LPM effect [35], both showers are likely to be contained within the detector volume. In charged current interactions of muon neutrino and antineutrinos we only use yE_ν for the shower energy, as we do in the neutral current (NC) interactions of all neutrino types. We use the GRV98 [36] structure functions to calculate the neutrino cross sections at ultra-high energy. The results are similar to those in Glück, Kretzer, and Reya [37] and to those calculated by Gandhi *et al.* [38] and Kwiecinski, Martin & Stasto [39].

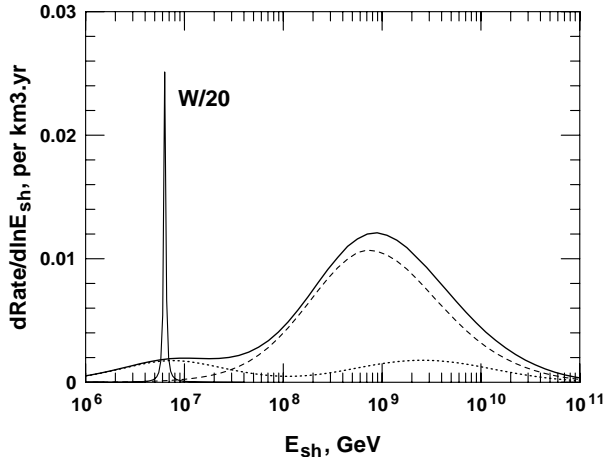


FIG. 10. Differential rates for showers initiated by charge current interactions of electron neutrinos (dashes) and antineutrinos (dots). The solid line gives the sum of those and the dash-dot lines gives the rate of the W^- resonance events. Absorption by the Earth is included so that at high energy the solid angle for detection is $\Omega \approx 2\pi$.

by charged current interactions of electron neutrinos and antineutrinos for a cosmological source evolution with $n = 3$. The total shower rate is dominated by ν_e interactions around the peak energy of the neutrino flux. As the interaction cross section increases with energy, the signal is dominated by showers with energy above 10^8 GeV . At this energy there is no significant background, either from neutrinos or muons, produced by cosmic ray interactions in the atmosphere. The spike at $E_\nu = 6.3 \times 10^6 \text{ GeV}$ is the rate for W^- boson production by $\bar{\nu}_e$ -electron interactions [40], divided by 20. The differential rate in the vicinity of the resonance is very high but the relevant energy range is small and the total rate is 0.03 per $\text{km}^3 \text{ yr}$. Accounting for invisible W^- decay modes would reduce the rate for showers even further.

Table I gives the shower rates per km^3 of water per yr for showers generated by different types of neutrino interactions and different flavors. These rates represent $d\sigma_\nu/dy$ folded with the flux of neutrinos reaching the detector and do not account for any experimental efficiency and detector biases. As such, they can only serve as an estimate of realistic event rates. The rates are low: the IceCube [41] and ANTARES [42] km^3 -size experiments may not expect to detect these neutrinos. In addition violation of any of the following assumptions may further decrease expectations

- (i) the detected ultra-high energy cosmic rays are not produced by a single nearby source,
- (ii) the powerful sources of ultra-high energy cosmic rays are homogeneously distributed in the Universe, and
- (iii) our normalization of the power of the cosmic ray sources and the injection spectrum are correct.

In case that only a fraction of the UHECR comes from homogeneously distributed sources, these rates come down to the same fraction of the values presented in Table I. On the other hand, for the cosmological evolution model with $n = 4$ the rates will go up by a factor of about 3, and assuming a cosmological constant with $\Omega_\Lambda = 0.7$ could give another moderate increase by a factor of 1.6 – 1.7.

TABLE I. Rates per km^3 water per year of showers above different energies generated by different types of neutrino interactions for $P_0 = 4.5 \times 10^{44} \text{ erg/Mpc}^3/\text{yr}$ and a cosmological evolution with $n = 3$ for homogeneously distributed cosmic ray sources (see text).

$\log E_{sh} \text{ (GeV)} >$	6	7	8	9	10
all ν , NC	0.052	0.046	0.032	0.008	0.001
ν_e , CC	0.054	0.051	0.046	0.024	0.004
$\nu_\mu + \nu_\tau$, CC	0.092	0.080	0.057	0.014	0.002
total	0.192	0.177	0.144	0.046	0.007

Fig. 10 shows the differential rate for showers initiated

The rates shown in Table I do not depend on the assumption that the atmospheric neutrino anomaly could be explained by oscillations of ν_μ into ν_τ [43]. On the very long astrophysical pathlength 50% of the muon neutrinos would be converted to tau neutrinos. Charge current interactions of ν_τ would not, however, be different from the ν_μ CC interactions and so their sum does not depend on oscillation parameters.

Another interesting process is the detection of τ 's produced in ν_τ CC interactions in the material surrounding the detector. Estimates show that the tau decay inside the detector will generate a signal which is comparable in shower energy and rate to that of ν_e CC interactions. Whether or not τ decays can be observed as separate events depends on the τ energy, which affects both decay length and energy loss [44], and the detector volume. A proper study of event rates for throughgoing or stopping τ and μ leptons depends on the detector geometry, location and surrounding material and is beyond the scope of this paper.

VI. DISCUSSION AND CONCLUSIONS

The biggest uncertainty in the magnitude of the neutrino fluxes from proton propagation is related to the distribution of cosmic ray sources. All arguments about the normalization of the cosmic ray injection power and the cosmological evolution of the cosmic ray sources are based on the assumption that the detected UHECR are of astrophysical origin and are not accelerated at a single nearby source. If the latter were the case, and the nearby source were responsible for all particles above 10^{19} eV, we should have to restrict the source distance to less than 20 Mpc [20]. The local ultra-high energy cosmic ray density would then be much higher than the average cosmic ray density in the Universe. There will be, no doubts, other regions where ultra-high energy cosmic rays are accelerated and are over-abundant. The overall normalization of the cosmic ray power would then depend on the filling factor of such regions. If one estimates this filling factor from the volume of the walls of galactic concentration, such as the supergalactic plane, that describes the galactic distribution within a redshift less than 0.05 [45], to nearby voids it will certainly not exceed 10%. In such a case the neutrino production due to proton propagation would be minimal as shown in Fig. 8 with the dotted line.

A correct estimate of the power in UHECR depends on the strength of the extragalactic magnetic field in our neighborhood. In case of an average strength of the turbulent field exceeding 1 nG, cosmic rays with an energy of about 10^{19} eV and below (with a gyroradius of less than 10 Mpc) will have diffusive propagation pattern, which will enhance their flux at Earth. On the other hand, regular extragalactic fields may guide these particles along the walls of matter concentration. All effects related to the propagation of UHECR should be a subject of fur-

ther investigation before we could give a more reliable estimate of the UHECR power.

Recently several authors have argued that powerful astrophysical systems and potential cosmic ray sources, such as GRB, have a cosmological evolution stronger than $(1+z)^3$ [29,46]. Ref. [29] presents a combined analysis of the far infrared luminosity as a tracer of the star formation rate [27] as a function of redshift and the gamma ray burst fluence. The star formation rate is fit with an exponential rise of $\exp(2.9z)$ to a redshift of 1.7 and the GRB fluence distribution suggests a slow decrease at higher z . The use of such strong cosmological evolution and high activity at redshifts higher than 2 would place the estimate of the neutrino flux halfway between the two cosmological evolution models shown in Fig. 9.

Another important factor is the injection spectrum of UHECR and the highest energy at acceleration. The qualitative picture of its influence is demonstrated in Fig. 1. Generally protons have to be accelerated to energies above 10^{20} eV to generate significant neutrino fluxes from their propagation. This threshold is reduced by $(1+z)$ for contributions from high redshift. In view of the observations of cosmic rays of energy significantly higher than 10^{20} eV this is very likely if the sources of these particles are astrophysical objects.

Assuming homogeneously distributed astrophysical sources we obtain a neutrino flux similar to the Waxman & Bahcall limit at neutrino energies above 10^{18} eV. This means that, with the assumptions and restrictions discussed above, one may expect similar fluxes of UHE neutrinos produced in astrophysical sources and in UHECR propagation.

Since the signature of these ultra-high energy neutrinos are showers, different types of air shower detectors should also be able to observe the highest end of the neutrino spectrum. The effective volume of the Auger observatory for UHE neutrino interactions was estimated to 30 km^3 of water equivalent [47]. If this effective volume was achieved for a shower energy of 10^{19} eV, the Auger observatory would see about 0.3 events per year from the estimates shown in Table I. It is interesting to note that at an energy of 10^{18} eV the τ decay length ($l_\tau = 49E/(10^{18}\text{eV}) \text{ km}$) is of the order of the dimensions of the Auger observatory. ‘Double bang’ events, caused by τ neutrinos as suggested by Learned & Pakvasa [48], could be detected if the sensitivity of the array was significant in this energy range.

As the effective volumes required are extremely large, the proposed satellite air shower experiments EUSO and OWL [49,50] might be well suited for the observation of ultra-high energy neutrino fluxes; however, with the current advertised threshold of 5×10^{19} eV most of the potential event rate would go undetected. Because of their large field of view, these detectors should in principle be able to observe ‘double bang’ events of energy above 10^{19} eV – if the threshold energy were lowered to that level.

Showers generated by ultra-high energy neutrinos could also be observed by their radio emission [51,52].

Prototype experiments are in operation [53] and suggestions have been made for full scale experiments [54,55] that would have an energy threshold of 10^{18} eV and a full effective volume of 10^2 - 10^4 km³. Such detectors could take advantage of the higher shower rate that corresponds to the maximum of the neutrino flux as shown in Fig. 10.

The potential detection of ultra-high energy neutrinos is a crucial experimental result that will help us distinguish between an astrophysical (acceleration) and cosmological (top-down) origin of UHECR. In top-down scenarios the neutrino fluxes are primary, roughly equal to the gamma ray fluxes and at least an order of magnitude above the ultra-high energy nucleon fluxes. In all astrophysical scenarios the neutrinos, due to cosmic ray interactions at their sources or in propagation, are secondary and their flux is a fraction of the cosmic ray flux.

Measuring neutrinos from CR propagation can also help to distinguish between protons and heavy nuclei, such as iron, as highest energy cosmic rays. The energy loss of heavy nuclei during propagation over cosmological distances is governed by photo-disintegration. The absorption of photons leads mainly to giant dipole resonance excitation of the nuclei and, with a high probability, subsequently to the emission of a single nucleon in the de-excitation process [56]. Hence the neutrino spectrum is expected to be dominated by relatively low-energy neutrinos ($E_\nu \lesssim 10^7$ GeV) from the beta decay of neutrons and unstable nuclei.

Finally it should be mentioned that the magnitude of the flux and the arrival direction of UHE neutrinos are a good indication of the cosmic ray source distribution in astrophysical scenarios.

ACKNOWLEDGMENTS

The authors acknowledge helpful discussions with T.K. Gaisser, R.J. Protheroe and F.W. Stecker. The research of TS is supported in part by NASA Grant NAG5-7009. RE is supported in part by the US Department of Energy contract DE-FG02 91ER 40626. These calculations are performed on DEC Alpha and Beowulf clusters funded by NSF grant PHY-9601834.

-
- [1] K. Greisen, Phys. Rev. Lett. **16**, 748 (1966); G.T. Zatsepin & V.A. Kuzmin, JETP Lett. **4**, 78 (1966).
 [2] V.S. Berezhinsky & G.T. Zatsepin, Phys. Lett. **28B**, 423 (1969); Sov. J. Nucl. Phys. **11**, 111 (1970).
 [3] J. Wdowczyk, W. Tkaczyk & A.W. Wolfendale, J. Phys. A **5**, 1419 (1972).
 [4] F.W. Stecker, Astroph. Space Sci. **20**, 47 (1973).
 [5] V.S. Berezhinsky & A.Yu. Smirnov, Astroph. Space Sci. **32**, 461 (1975).
 [6] V.S. Berezhinsky & G.T. Zatsepin, Sov. J. Uspekhi, **20**, 361 (1977).
 [7] F.W. Stecker, Ap. J. **238**, 919 (1979).
 [8] C.T. Hill & D.N. Schramm, Phys. Rev. D **31**, 564 (1985).
 [9] C.T. Hill, D.N. Schramm & T.P. Walker, Phys. Rev. D **34**, 1622 (1986).
 [10] G. Cunningham *et al.*, Ap. J. **236**, L1 (1980).
 [11] R.M. Baltrusaitis *et al.*, Phys. Rev. Lett. **54**, 1875 (1985).
 [12] F.W. Stecker *et al.*, Phys. Rev. Lett. **66**, 2697 (1991).
 [13] S. Yoshida & M. Teshima M., Progr. Theor. Physics **89**, 833 (1993).
 [14] R.J. Protheroe & P.A. Johnson, Astropart. Phys. **4**, 253 (1996).
 [15] M. Nagano & A.A. Watson, Rev. Mod. Phys. **72**, 690 (2000).
 [16] D. Bird *et al.*, Ap. J. **441**, 144 (1995).
 [17] N. Hayashida *et al.*, Phys. Rev. Lett. **73**, 3491 (1994).
 [18] V.S. Berezhinsky, M. Kachelriess & A. Vilenkin, Phys. Rev. Lett. **79**, 4302 (1997).
 [19] A. Bhattacharjee & G. Sigl, Phys. Rep. **327**, 109 (2000).
 [20] T. Stanev *et al.*, Phys. Rev. D **62**, 093005 (2000).
 [21] A. Mücke *et al.*, Comp. Phys. Comm. **124**, 290 (2000).
 [22] A.V. Olinto, Phys. Rept. **333-4**, 329 (2000).
 [23] T.K. Gaisser, in Proc. of High Energy Gamma Ray Astronomy, ed. F.A. Aharonian and H.J. Völk, AIP Conf. Proc. 558, 27 (2001).
 [24] E. Waxman, Ap. J. **452**, L1 (1995)
 [25] E. Waxman & J. Bahcall, Phys. Rev. D **59**, 023002 (1999).
 [26] J. Bahcall & E. Waxman, astro-ph/9902383.
 [27] P. Madau *et al.*, Mon. Not. R. Astr. Soc. **238**, 1388 (1996).
 [28] M. Schmidt, Ap. J. **523**, L117 (1999); E.E. Fenimore & E. Ramirez-Ruiz, astro-ph/0004176.
 [29] G. Pugliese *et al.*, A&A **358**, 409 (2000).
 [30] J.A. Peacock, MNRAS **217**, 601 (1985).
 [31] J.P. Rachen & P.L. Biermann, A&A **272**, 161 (1993).
 [32] M. Blanton, P. Blasi & A.V. Olinto, Astropart. Phys. **15**, 275 (2001).
 [33] N.A. Bahcall *et al.*, Science **248**, 1481 (1999).
 [34] S.M. Carroll, Living Rev. Rel. **4**, 1 (2001).
 [35] J. Alvarez-Muniz and E. Zas, Phys. Lett. **B411**, 218 (1997); Phys. Lett. **B434**, 396 (1998).
 [36] M. Glück, E. Reya & A. Vogt, Eur. Phys. J. **C5**, 461 (1998).
 [37] Glück, M., S. Kretzer, and E. Reya, Astropart. Phys. **11**, 327 (1999).
 [38] R. Gandhi *et al.*, Phys. Rev. D **58**, 093009 (1998).
 [39] J. Kwiecinski, A.D. Martin and A.M. Stasto, Phys. Rev. D **59**, 093002 (1999).
 [40] S.L. Glashow, Phys. Rev. **118B**, 316 (1960).
 [41] IceCube proposal, <http://pheno.physics.wisc.edu/icecube> (see also <http://www.ssec.wisc.edu/a3ri/icecube/>).
 [42] ANTARES Collab., E. Aslanides *et al.*, astro-ph/9907432.
 [43] T. Kajita & Y. Totsuka, Rev. Mod. Phys. **73**, 85 (2001).
 [44] S.I. Dutta *et al.*, Phys. Rev. D **63**, 094020 (2001).
 [45] O. Lahav *et al.*, Mon. Not. R. Astr. Soc. **312**, 166 (2000).
 [46] S.T. Scully & F.W. Stecker, astro-ph/0006112.

- [47] K.S. Capelle *et al.*, *Astropart. Phys.* **8**, 321 (1998)
- [48] J.G. Learned & S. Pakvasa, *Astropart. Phys.* **3**, 267 (1995).
- [49] The current status of the EUSO proposal is displayed at www.ifcai.pa.cnr.it.
- [50] L. Scarsi *et al.* in Proc. 26th ICRC (Salt Lake City), **2**, 384 (1999).
- [51] E. Zas, F. Halzen and T. Stanev, *Phys. Rev. D* **45**, 362 (1992).
- [52] G. Frichter, J. Ralston and D. McKay, *Phys. Rev. D* **53**, 1684 (1996).
- [53] D. Besson *et al.* in Proc. 26th ICRC (Salt Lake City), **2**, 467 (1999).
- [54] D. Seckel and G. Frichter, Proc. 26th Int. Cos. Ray Conf., Salt Lake City (1999).
- [55] D. Seckel, astro-ph/0103300, in Proc. Radio Detection of High Energy Particles, UCLA, Los Angeles (2000).
- [56] J. P. Rachen, PhD-thesis, MPIfR Bonn, Germany, 1996.